Volume 60
Number 46
11 June 2024
Pages 5881–5990

ChemComm

Chemical Communications

rsc.li/chemcomm

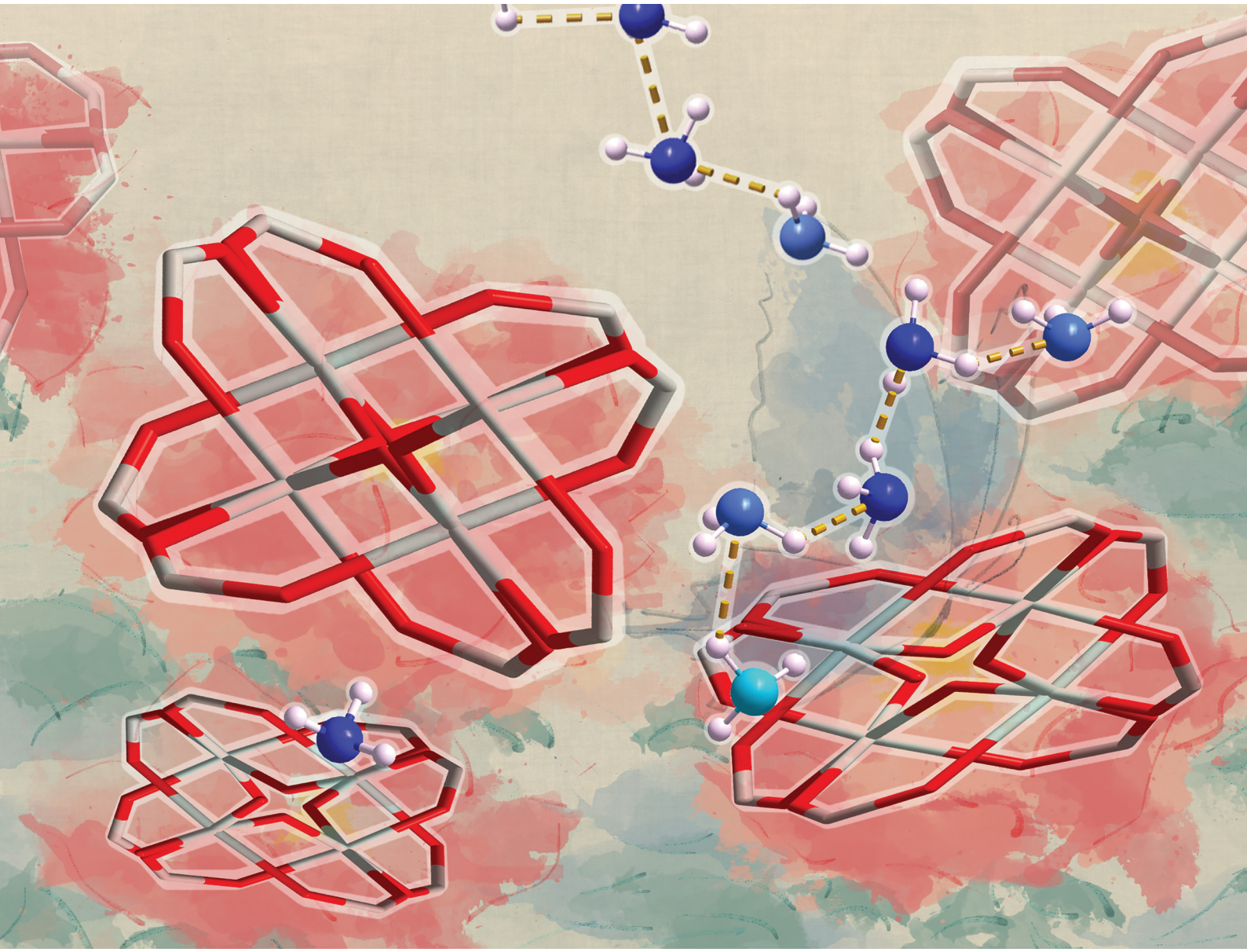

ISSN 1359-7345

ROYAL SOCIETY OF CHEMISTRY

COMMUNICATION

Martin Schröder, Sihai Yang *et al.*
High adsorption of ammonia in a titanium-based metal–organic framework

60 YEARS ANNIVERSARY

ChemComm

COMMUNICATION

View Article Online
View Journal | View Issue

Cite this: *Chem. Commun.*, 2024, **60**, 5912

Received 29th March 2024,
Accepted 25th April 2024

DOI: 10.1039/d4cc01449a

rsc.li/chemcomm

High adsorption of ammonia in a titanium-based metal–organic framework†

Xiangdi Zeng,[a] Jiangnan Li,[ab] Meng He,[a] Wanpeng Lu,[a] Danielle Crawshaw,[a] Lixia Guo,[ab] Yujie Ma,[a] Meredydd Kippax-Jones,[ac] Yongqiang Cheng,[d] Pascal Manuel,[e] Svemir Rudić,[e] Mark D. Frogley,[c] Martin Schröder *[a] and Sihai Yang *[ab]

We report the high adsorption of NH_3 in a titanium-based metal–organic framework, MFM-300(Ti), comprising extended $[TiO_6]_\infty$ chains linked by biphenyl-3,3′,5,5′-tetracarboxylate ligands. At 273 K and 1 bar, MFM-300(Ti) shows an exceptional NH_3 uptake of 23.4 mmol g^{-1} with a record-high packing density of 0.84 g cm^{-3}. Dynamic breakthrough experiments confirm the excellent uptake and separation of NH_3 at low concentration (1000 ppm). The combination of *in situ* neutron powder diffraction and spectroscopic studies reveal strong, yet reversible binding interactions of NH_3 to the framework oxygen sites.

Ammonia (NH_3) is an important feedstock that is produced at a scale of *ca.* 150 million tonnes per year.[1] In addition, the high volumetric (~0.105 kg L^{-1}) and gravimetric (17.7 wt%) hydrogen densities of NH_3 make it a promising renewable fuel and a potential hydrogen carrier for on-board storage. However, the highly toxic and corrosive nature of NH_3 poses challenges in its safe storage and transportation. At present, NH_3 is transported as a compressed liquid either at 10 bar at 25 °C or at ambient pressures at low temperature (liquefication point of −33 °C).[2] Thus, the development of robust sorbents for reversible NH_3 adsorption under mild conditions is of great importance.

Porous materials, such as zeolites,[3] active carbons,[4] mesoporous silica,[5] and organic polymers[6] have been tested for NH_3 adsorption. However, these materials demonstrate limited capacities; for example, 9.3 mmol g^{-1} in 13X zeolite,[3] 8.8 mmol g^{-1} in MCM-41,[5] and 11.4 mmol g^{-1} in Amberlyst 15.[7] Metal–organic frameworks (MOFs) have demonstrated potential for NH_3 adsorption[8] owing to their high accessible surface area, and their tailored porosity and pore environment. The MOFs displaying top performance for NH_3 adsorption are primarily divalent/trivalent-based MOFs or MOF composites, such as LiCl@MIL-53-$(OH)_2$[9] (33.9 mmol g^{-1} at 298 K and 1 bar) and Ni_acryl_TMA[10] (23.5 mmol g^{-1} at 298 K and 1 bar). However, the stability of MOFs toward NH_3 adsorption needs to be improved, and typically tetravalent metal-based MOFs (*e.g.*, Zr^{4+}, V^{4+}, Hf^{4+}) exhibit enhanced thermal and chemical stability. However, the reported Zr-based MOFs show limited NH_3 adsorption capacities (8.40 mmol g^{-1} in UiO-67[11]). On the other hand, the study of V-based MFM-300(V) for NH_3 adsorption has revealed that the incorporation of V^{4+} can effectively enhance the NH_3 adsorption,[12] which is attributed to the charge transfer within the framework and the formation of N_2H_4.

Herein, we report a novel Ti^{4+}-based MOF, MFM-300(Ti) $[Ti_2(O)_2(C_{16}H_6O_8)]$, which displays a reversible NH_3 uptake of 23.4 mmol g^{-1} at 273 K and 1 bar, among the best NH_3 sorbent materials showing reversible adsorption to date. Significantly, the packing density of NH_3 in MFM-300(Ti) (0.84 g cm^{-3}, calculated using the pore volume derived from crystallographic data) is comparable to that of solid NH_3 at −80 °C (0.82 g cm^{-3}), due to the strong guest–guest interaction within the pores. In addition, breakthrough experiments confirm that MFM-300(Ti) can effectively capture and separate NH_3 at low concentrations (1000 ppm). The binding sites of NH_3 in MFM-300(Ti) have been determined by *in situ* neutron powder diffraction (NPD), and its binding dynamics investigated by a combination of *in situ* inelastic neutron scattering (INS) and synchrotron IR microspectroscopy.

Solvated MFM-300(Ti), $[Ti_2(O)_2(C_{16}H_6O_8)(H_2O)_2(C_3H_6O)_{0.7}]$, was prepared *via* a solvothermal reaction of {Ti_8AF} clusters,[13] H_4L (biphenyl-3,3′,5,5′-tetracarboxylic acid, H_4bptc), acetic acid, acetic anhydride and methanol at 180 °C for 12 h. Structure solution by NPD (Fig. 1a and b) confirms that MFM-300(Ti) crystallises in the tetragonal space group $I4_122$ and is isostructural to other MFM-300 materials.[14] The presence of *cis*-μ_2-O moieties rather than *cis*-μ_2-OH groups as

[a] *Department of Chemistry, University of Manchester, Manchester, M13 9PL, UK. E-mail: M.Schroder@manchester.ac.uk, Sihai.Yang@manchester.ac.uk*
[b] *College of Chemistry and Molecular Engineering, Beijing National Laboratory for Molecular Sciences, Peking University, Beijing, 100871, China. E-mail: Sihai.Yang@pku.edu.cn*
[c] *Diamond Light Source, Harwell Science Campus, Oxfordshire, OX11 0DE, UK*
[d] *Neutron Scattering Division, Neutron Sciences Directorate, Oak Ridge National Laboratory, Oak Ridge, TN 37831, USA*
[e] *ISIS Neutron and Muon Facility, Rutherford Appleton Laboratory, Didcot, OX11 0QX, UK*

† Electronic supplementary information (ESI) available. CCDC 2296493, 2296494 and 2296495. For ESI and crystallographic data in CIF or other electronic format see DOI: https://doi.org/10.1039/d4cc01449a

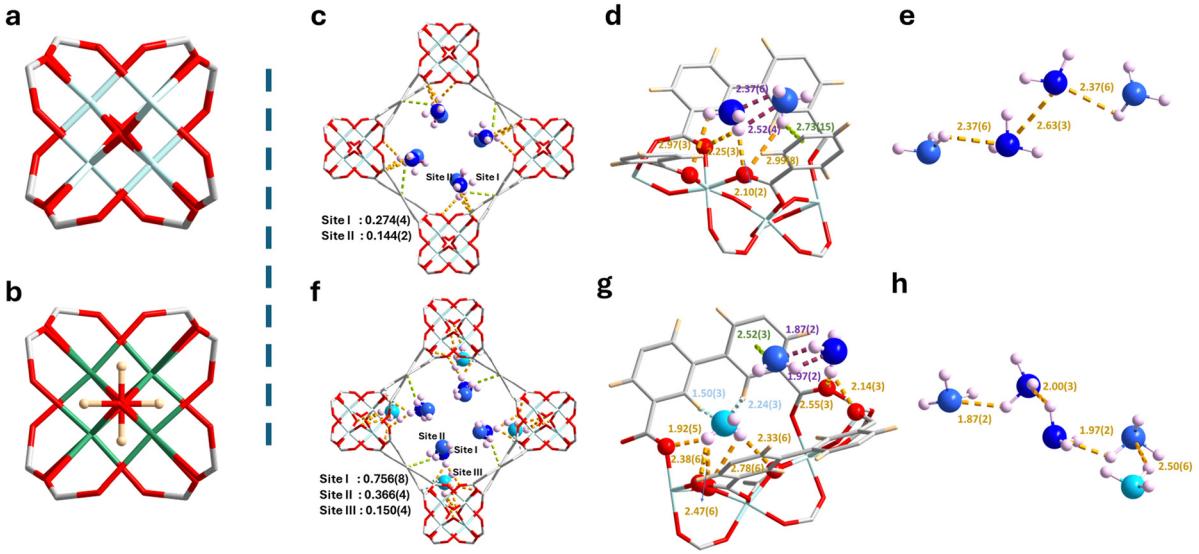

Fig. 1 Views of crystal structures of bare and ND_3-loaded MFM-300(Ti) as determined by NPD at 10 K. The occupancy of each site has been converted to ND_3/Ti for clarity. (a) and (b) Views of MFM-300(Ti) and MFM-300(M^{III}) along the *c*-axis, respectively. (c) and (f) Views of packing of ND_3 in MFM-300(Ti) along the *c*-axis in MFM-300(Ti)·0.84 ND_3 and MFM-300(Ti)·2.54 ND_3, respectively. (d) and (g) Detailed views of host–guest interactions in MFM-300(Ti)·0.84 ND_3 and MFM-300(Ti)·2.54 ND_3, respectively. (e) and (h) Guest–guest interaction along *c*-axis in MFM-300(Ti)·0.84 ND_3 and MFM-300(Ti)·2.54 ND_3, respectively. Colour code for atoms: Ti, turquoise; O, red; C, grey; H, tan; N, blue (dark blue, blue, and light blue for site I, II, and III, respectively); D, purple.

observed in M^{3+}-based analogues is confirmed by NPD and FTIR spectra (Fig. 1a and b, Fig. S7, ESI†). MFM-300(Ti) exhibits an open framework structure comprising of chains of $[TiO_4(O)_2]$ moieties bridged by tetracarboxylate ligands L^{4-} to afford 1D channels along the *c* axis with a diameter of 7.4 Å. Desolvated MFM-300(Ti) displays a Brunauer–Emmett–Teller (BET) surface area of 890 $m^2\ g^{-1}$ and pore volume of 0.44 $cm^3\ g^{-1}$, as determined from the CO_2 isotherm at 195 K (Fig. S1, ESI†), consistent with the porosity derived from the crystal structure (pore volume of 0.45 $cm^3\ g^{-1}$). Crystallites of MFM-300(Ti) show rod-like morphology (Fig. S2, ESI†). The excellent thermal stability up to 450 °C and the chemical stability of MFM-300(Ti) has been confirmed by thermogravimetric analysis (TGA; Fig. S3, ESI†), variable temperature powder X-ray diffraction (VT-PXRD; Fig. S4, ESI†), PXRD analysis of samples soaked in various solutions (Fig. 1c and Fig. S5, ESI†), and the CO_2 adsorption measurements for samples after various treatments to confirm the porosity (Fig. S6, ESI†).

The adsorption isotherms for NH_3 in MFM-300(Ti) were measured between 273 and 308 K at 1 bar (Fig. 2a). MFM-300(Ti) exhibits an exceptional and fully reversible NH_3 uptake of 23.4 mmol g^{-1} at 273 K and 1.0 bar, comparable to state-of-the-art sorbents (Table S1, ESI† and Fig. 2e). Hysteresis in the NH_3 isotherms was observed at all temperatures, indicating the presence of strong host–guest interactions. The pressure-swing experiment was conducted at 298 K from 0 to 0.1 bar. Little change in sorption capacity or structure was observed for MFM-300(Ti) after 25 cycles of adsorption and desorption of NH_3 (Fig. 2b and c), confirming the excellent stability of MFM-300(Ti) towards NH_3. The residual NH_3 observed on desorption during cyclic pressure-swing experiments suggests the presence of strong binding sites in the pore, consistent with the observed hysteresis. The dynamic NH_3 uptake of MFM-300(Ti) at low concentration (1000 ppm) was recorded as 0.6 mmol g^{-1} at 298 K, demonstrating an excellent capture capability (Fig. 2d). The heat of adsorption (Q_{st}) of NH_3 in MFM-300(Ti) was calculated to be 39–52 kJ mol^{-1} (Fig. 2f and Table S2, ESI†), comparable with other MOFs incorporating strong binding sites, such as UiO-66Cu(II)[15] (25–55 kJ mol^{-1}).

In situ NPD data for ND_3-loaded MFM-300(Ti) were collected at 10 K (ND_3/Ti = 0.42, 1.27), and Rietveld refinements afforded distinct binding sites for ND_3. At low-loading (ND_3/Ti = 0.42; MFM-300(Ti)·0.84 ND_3) (Fig. 1c and d), two binding sites (I and II) are observed. Site I is anchored by hydrogen bonding between the ND_3 molecules and the carboxylate oxygen atoms [$ND_3\cdots O_{ligand}$ = 2.10(2)–2.97(3) Å]. Site II is adjacent to site I, stabilised by hydrogen bonding interactions [$ND_3\cdots O_{ligand}$ = 2.99(8) Å], electrostatic interactions [$ND_3\cdots$aromatic rings = 2.52(3)–2.73(15) Å], and guest–guest interactions [$ND_3\cdots ND_3$ = 1.87(2)–2.52(4) Å]. Interestingly, when the loading was increased to 1.27 ND_3/Ti (MFM-300(Ti)·2.54 ND_3) (Fig. 2e and f), an additional binding site was observed even closer to the $[TiO_6]_\infty$ chain and stabilised by multiple supramolecular interactions [$C\text{–}H_{aromatic}\cdots N$ = 1.50(3)–2.24(3) Å, $ND_3\cdots O_{ligand}$ = 1.92(5)–2.38(6) Å, and $ND_3\cdots O_{bridge}$ = 2.33(6)–2.78(6) Å]. In addition, the adsorbed ND_3 molecules propagated to form a 1D network within the channel of MFM-300(Ti) (Fig. 1e and h). Moreover, the hydrogen bonding distance [$N\text{–}D\cdots N$ = 2.37(6)–2.52(3) Å] between adsorbed ND_3 molecules in MFM-300(Ti)·0.84 ND_3 decreases to [$N\text{–}D\cdots N$ = 1.87(3)–2.00(3) Å] in MFM-300(Ti)·2.54 ND_3. This tighter host–guest and guest–guest interaction with increasing NH_3 loading is consistent with the trend of Q_{st} (Fig. 2f). Notably, the shortest distance between adsorbed ND_3 molecules in MFM-300(Ti) is 1.87 Å, which is notably shorter than those previously observed [2.33 Å in MFM-300(Fe); 3.05 Å in

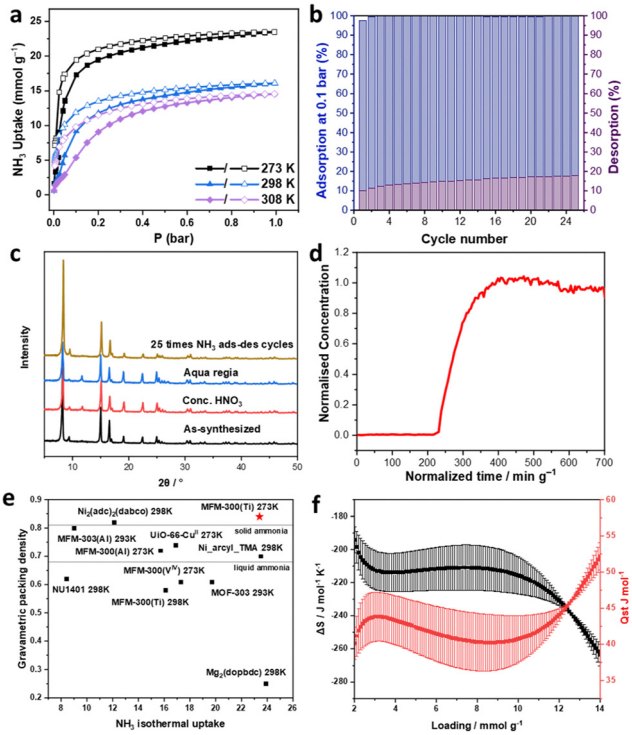

Fig. 2 (a) Adsorption isotherms of NH_3 in MFM-300(Ti) at 273–308 K up to 1.0 bar (adsorption, solid symbols; desorption, open symbols). (b) Cyclic adsorption–desorption of NH_3 in MFM-300(Ti) at 298 K between 0 and 0.1 bar; dark-coloured bars show the residual NH_3 within the MOF upon pressure-swing desorption at 298 K. (c) PXRD patterns of MFM-300(Ti), (black: as-synthesised, red: after soaking in concentrated HNO_3 for one day, blue: after soaking in aqua regia for one day, dark yellow: after 25 adsorption–desorption cycles). (d) Breakthrough experiment for NH_3 (1000 ppm diluted in He) through a fixed-bed packed with MFM-300(Ti). (e) Plot of NH_3 isothermal adsorption capacities and NH_3 packing density in stable MOF materials (f) isosteric enthalpy and entropy of adsorption for MFM-300(Ti) at different NH_3 loadings.

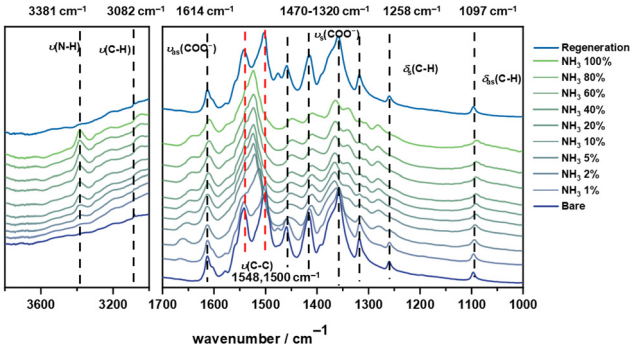

Fig. 3 *In situ* synchrotron FT-IR spectra of MFM-300(Ti) as a function of NH_3 adsorption and of regenerated MFM-300(Ti) under a flow of dry N_2 at 100 mL min^{-1} at 298 K for 2 h.

MFM-300(V^{IV})][15] and reflects highly efficient packing of NH_3 molecules in MFM-300(Ti), consistent with the high packing density derived from the adsorption isotherms. Compared with MFM-300(M^{III}),[15] the replacement of μ_2-OH by μ_2-O in MFM-300(Ti) reduces the steric hindrance between the bridging hydroxyl groups and guest molecules, providing additional binding sites and boosting the storage of NH_3. In MFM-300(V^{IV}), the presence of the vanadium centre promotes charge transfer between NH_3 molecules, resulting in the observation of both N_2D_4 and ND_4^+ molecules in the pore,[15] which limits the reusability of the MOF. The utilisation of Ti^{4+} ions not only improves the structural stability of the material, but also hinders charge transfer to enhance the adsorption reversibility of NH_3.

The dynamics of host–guest binding has been analysed using *in situ* synchrotron IR microspectroscopy, INS, and density functional theory (DFT) calculations. The absence of the characteristic IR band of hydroxyl group at ~3600 cm^{-1} in activated MFM-300(Ti) (Fig. S7, ESI†) confirmed the presence of *cis*-μ_2-O as a result of the tetravalent Ti^{4+} sites, consistent with the NPD analysis. On loading NH_3, a new band at 3381 cm^{-1} assigned to a ν(N–H) stretching vibration is observed, confirming the adsorption in the framework (Fig. 3). The band at 1614 cm^{-1} can be assigned to $\nu_{as}(COO^-)$, which broadens on loading of NH_3. The bands at 1470 cm^{-1}, 1414 cm^{-1},1360 cm^{-1}, and 1320 cm^{-1} can be assigned to different vibrations $\nu_s(COO^-)$ of the carboxylate group in the framework, and all show red-shifts on increasing loading of NH_3. This suggests the presence of strong interactions between NH_3 and the carboxylate groups of the bridging ligand. Simultaneously, as the concentration of NH_3 increases from 2% to 5%, two bands at 1548 and 1500 cm^{-1} corresponding to aromatic C–C stretching vibrations merge into one band (1525 cm^{-1}), which is not observed in other MFM-300 materials. This indicates a notable change in the conjugated structure of the aromatic rings, which is further evidenced by the elongation of the C–C bonds in the biphenyl linker from 1.458(2) Å in bare MFM-300(Ti) to ~1.497(4) Å in MFM-300(Ti)·0.84 ND_3 and further to ~1.500(7) Å in MFM-300(Ti)·2.54 ND_3, as determined by the NPD analysis (Table S9, ESI†).

A combination of INS and DFT calculations has been employed to elucidate the dynamic behaviour of adsorbed NH_3 within MFM-300(Ti). The congruence between experimental and simulated INS spectra for MFM-300(Ti) (Fig. S12, ESI†) and NH_3-loaded MFM-300(Ti) (Fig. S13, ESI†) is remarkable, allowing the assignments of INS peaks. Distinct peaks were observed in the INS difference spectra, which were obtained by subtracting the features of the bare MFM-300(Ti) and the sample cell from the spectra of NH_3-loaded MFM-300 (Ti) (Fig. 4b). Translational and rotational modes of adsorbed NH_3 molecules around its C_3 axis are observed between 4.4–14.4 meV and 16.6–23.5 meV, respectively. The bands at 26.5–41.7 meV correspond to the rocking motions of NH_3 around the N centre (Fig. 4c and d). In comparison to the spectrum of NH_3 in the solid state, where each NH_3 molecule forms a 3D hydrogen bonding network with six adjacent NH_3 molecules, the bands in all regions for adsorbed NH_3 exhibit shifts to lower energy and display broader features (for solid NH_3, 6.3–23.1 meV translational modes; 27.6–35.5 meV rotational modes; 36.7–56.9 meV rocking modes) (Fig. 4a). This phenomenon suggests a more dynamic environment for the adsorbed NH_3 molecules within MFM-300(Ti). Specifically, the

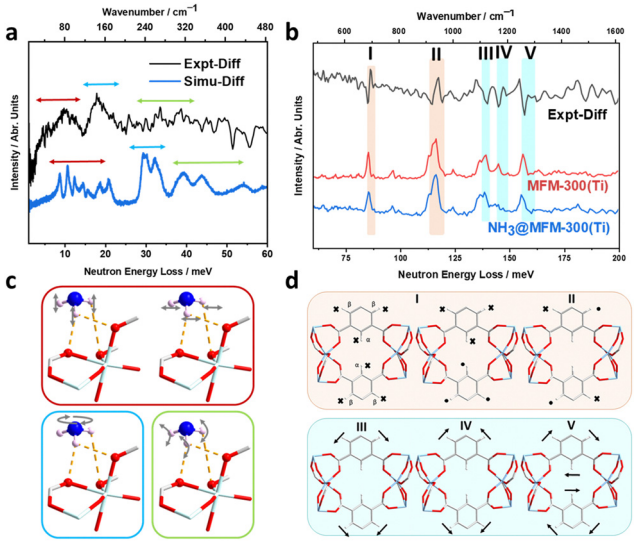

Fig. 4 Views of *in situ* INS spectra and the corresponding vibrational modes for MFM-300(Ti), before and after adsorption of NH_3. Difference spectra were obtained by subtraction of the INS spectra of the bare MOF from that for the NH_3-loaded MOF and are marked as Expt-Diff (experimental difference spectra). (a) Comparison of vibrational modes between solid NH_3 at 10 K (4.4–14.4 meV translational modes; 16.6–23.5 meV rotational modes; 26.5–41.7 meV rocking modes). (b) Experimental difference INS spectra for MFM-300(Ti) upon adsorption of NH_3 in the higher energy range. The scale factor for difference spectrum is 3. (c) and (d) Selected vibrational modes of confined NH_3 molecule and MFM-300(Ti).

rotational modes show more significant red shifts, attributed to the higher rotational flexibility of NH_3 in its adsorbed environment in MFM-300(Ti).

The vibrational features of the framework have been observed in the high energy region of the difference-INS spectra. Features at (I) 84.9, (II) 117.6, (III) 126.5, (IV) 145.1, and (V) 155.9 meV can be assigned to C–H out-of-C_6-plane wagging (in-phase along the ring, meaning H atoms move in the same direction), C–H out-of-C_6-plane twisting (anti-phase along the ring, meaning neighbouring H atoms move in opposite directions), C–H in-C_6-plane scissoring mode, in phase, C–H in-C_6-phane scissoring mode, anti-phase, and C–H in-C_6-plane rocking mode, respectively (Fig. 4b and d). Compared with other MFM-300(M) materials, MFM-300(Ti) shows more versatile C–H bending modes, and the changes in the C–H bending peaks upon adsorption of NH_3 indicate the strong host–guest interactions between the benzyl ring of the framework and NH_3 molecules. These results are in excellent agreement with the NPD and FTIR study.

In summary, we report the high capacity and reversible adsorption of NH_3 within a novel titanium-based MOF, MFM-300(Ti). This framework features a unique structure composed of extended $[TiO_6]_\infty$ chains linked by tetra-topic ligands $[(C_{16}H_6O_8)^{4-}]$. Notably, at 273 K and 1 bar, MFM-300(Ti) shows an exceptional NH_3 uptake of 23.4 mmol g^{-1} and a record-high packing density of 0.84 g cm^{-3}. The volumetric and gravimetric adsorption capacity is 0.36 g cm^{-3} and 0.28 g g^{-1}, respectively. Dynamic breakthrough experiments confirm excellent adsorption of NH_3 at low concentration (1000 ppm). The combination of *in situ* NPD, INS, FTIR and DFT studies reveal the molecular details on the host–guest binding interactions. This study has established MFM-300(Ti) as a highly efficient sorbent for NH_3, demonstrating its potential for practical applications.

We thank EPSRC (EP/I011870, EP/V056409), University of Manchester, National Science Foundation of China and BNLMS for funding. This project has received funding from the European Research Council (ERC) under the European Union Horizon 2020 research and innovation programme (grant agreement no. 742401, NANOCHEM and PoC665632). We are grateful to the STFC/ISIS Facility and Diamond Light Source for access to beamlines WISH/TOSCA and B22 (SM30398), respectively. The computing resources were made available through the VirtuES and the ICE-MAN projects, funded by Laboratory Directed Research and Development program and Compute and Data Environment for Science (CADES) at ORNL.

Conflicts of interest

There are no conflicts to declare.

Notes and references

1 NITROGEN (FIXED)—AMMONIA U.S. Geological Survey, Mineral Commodity Summaries, 2022, https://pubs.usgs.gov/periodicals/mcs2022/mcs2022-nitrogen.pdf.
2 D. R. MacFarlane, P. V. Cherepanov, J. Choi, B. H. Suryanto, R. Y. Hodgetts, J. M. Bakker, F. M. F. Vallana and A. N. Simonov, *Joule*, 2020, **4**, 1186–1205.
3 J. Helminen, J. Helenius, E. Paatero and I. Turunen, *AIChE J.*, 2000, **46**, 1541–1555.
4 T. Zeng, H. Huang, N. Kobayashi and J. Li, *Nat. Resour.*, 2017, **8**, 611–631.
5 A. M. B. Furtado, Y. Wang, T. G. Glover and M. D. LeVan, *Microporous Mesoporous Mater.*, 2011, **142**, 730–739.
6 C. J. Doonan, D. J. Tranchemontagne, T. G. Glover, J. R. Hunt and O. M. Yaghi, *Nat. Chem.*, 2010, **2**, 235–238.
7 J. Helminen, J. Helenius, E. Paatero and I. Turunen, *J. Chem. Eng. Data*, 2001, **46**, 391–399.
8 X. Han, S. Yang and M. Schröder, *J. Am. Chem. Soc.*, 2023, **145**, 1998–2012.
9 Y. Shi, Z. Wang, Z. Li, H. Wang, D. Xiong, J. Qiu, X. Tian, G. Feng and J. Wang, *Angew. Chem., Int. Ed.*, 2022, **61**, e202212032.
10 D. W. Kim, D. W. Kang, M. Kang, D. S. Choi, H. Yun, S. Y. Kim, S. M. Lee, J.-H. Lee and C. S. Hong, *J. Am. Chem. Soc.*, 2022, **144**, 9672–9683.
11 T. Yoskamtorn, P. Zhao, X.-P. Wu, K. Purchase, F. Orlandi, P. Manuel, J. Taylor, Y. Li, S. Day, L. Ye, C. C. Tang, Y. Zhao and S. C. E. Tsang, *J. Am. Chem. Soc.*, 2021, **143**, 3205–3218.
12 X. Han, W. Lu, Y. Chen, I. Da Silva, J. Li, L. Lin, W. Li, A. M. Sheveleva, H. G. Godfrey, Z. Lu, F. Tuna, E. J. L. McInnes, Y. Cheng, L. L. Daemen, L. J. M. McPherson, S. J. Teat, M. D. Frogley, S. Rudić, P. Manuel, A. J. Ramirez-Cuesta, S. Yang and M. Schröder, *J. Am. Chem. Soc.*, 2021, **143**, 3153–3161.
13 S. Wang, M. Cabrero-Antonino, S. Navalón, C.-C. Cao, A. Tissot, I. Dovgaliuk, J. Marrot, C. Martineau-Corcos, L. Yu, H. Wang, W. Shepard, H. García and C. Serre, *Chem*, 2020, **6**, 3409–3427.
14 S. Yang, J. Sun, A. J. Ramirez-Cuesta, S. K. Callear, W. I. David, D. P. Anderson, R. Newby, A. J. Blake, J. E. Parker, C. C. Tang and M. Schröder, *Nat. Chem.*, 2012, **4**, 887–894.
15 Y. Ma, W. Lu, X. Han, Y. Chen, I. Da Silva, D. Lee, A. M. Sheveleva, Z. Wang, J. Li, W. Li, M. Fan, S. Xu, F. Tuna, E. J. L. McInnes, Y. Cheng, S. Rudić, P. Manuel, M. D. Frogley, A. J. Ramirez-Cuesta, M. Schröder and S. Yang, *J. Am. Chem. Soc.*, 2022, **144**, 8624–8632.